Eur. Phys. J. C 54, 475–481 (2008)
DOI 10.1140/epjc/s10052-008-0536-3

THE EUROPEAN PHYSICAL JOURNAL C

Regular Article – Theoretical Physics

Revisiting glueball wave functions at zero and finite temperature

M. Loan[a]

[1] International School, Jinan University, Huangpu Road West, Guangzhou 510632, P.R. China
[2] School of Physics, The University of New South Wales, Kensington, Sydney, NSW 2052, Australia

Received: 6 October 2007 / Revised version: 11 December 2007 /
Published online: 31 January 2008 –

Abstract. We study the sizes and thermal properties of glueballs in a three-dimensional compact Abelian gauge model on improved lattice. We predict the radii of ~ 0.60 and ~ 1.12 in the units of string tension, or ~ 0.28 and ~ 0.52 fm, for the scalar and tensor glueballs, respectively. We perform a well controlled extrapolation of the radii to the continuum limit and observe that our results agree with the predicted values. Using Monte Carlo simulations, we extract the pole mass of the lowest scalar and tensor glueballs from the temporal correlators at finite temperature. We see clear evidence of the deconfined phase, and the transition appears to be similar to that of the two-dimensional XY model as expected from universality arguments. Our results show no significant changes in the glueball wave functions and masses in the deconfined phase.

PACS. 11.15.Ha; 12.38.Gc; 11.15.Me

1 Introduction

The prediction of glueball masses has since long been attempted in lattice gauge theory calculations [1–7]. These calculations show that the lowest-lying scalar, tensor and axial vector glueballs lie in the mass region of 1–2.5 GeV. While there is a long history of glueball mass calculations in lattice QCD, little is known about the glueballs besides their masses. Accurate lattice calculations of their size, matrix elements and form factors would help considerably in their experimental identification.

Glueball wave functions and sizes have been studied in the past [8–11], but much of the early work contains uncontrolled systematic errors, most notably from discretisation effects. The scalar glueball is particularly susceptible to such errors for the Wilson gauge action, due to the presence of a critical end point of a line of phase transitions in the fundamental-adjoint coupling plane. As this critical end point (which defines the continuum limit of a ϕ^4 scalar field theory) is neared, the coherence length in the scalar channel becomes large, which means that the mass gap in this channel becomes small; glueballs in other channels seem to be affected very little. Results in which the scalar glueball was found to be significantly smaller than the tensor were most likely due to contamination of the scalar glueball from this non-QCD critical point [9]. On the other hand, the calculations using operator overlaps obtained from variational optimization for improved lattice gauge action, which are designed to avoid spurious critical points, show that the scalar and tensor glueballs were of typical hadronic dimensions [1, 2, 11]. A straightforward procedure to address the controversy over glueball size is to measure the glueball wave function, much in the same way as the meson and baryon wave functions were measured [12].

In this paper, we study the low-lying scalar and tensor glueballs and their wave functions with a renormalized tadpole improved Symanzik gauge action [13]. Our techniques for calculating the glueball wave functions from Wilson loop operators are outlined in Sect. 2. We present and discuss our results at zero temperature in Sect. 3. We extend our method to examine the wave functions and masses at finite temperature in this section. Here we give an explicit interpretation of deconfinement in terms of the power-law behaviour of the correlation function. Section 4 is devoted to the summary and concluding remarks.

2 Wave functions of glueballs

In contrast with the techniques used in [9], we measure our lattice operators from spatially connected Wilson loops. Glueballs are colour-singlet states and one should be able to construct them with closed-loop paths that are gauge invariant. The choice of such loops eliminate the need for gauge fixing[1]. Although the calculations in [9] have pro-

[a] e-mail: mushe@phys.unsw.edu.au

[1] It should be noted that gauge-invariant Wilson loops have an a^4 dependence, to be compared to the a^2 dependence of

duced some interesting results, the approach suffers from a basic problem: the observables are calculated from a lattice version of the 2-glue operator, which risks a mixture of glueball states with flux states[2].

In this study we take a more direct approach to the problem. We measure the observables in a three-step procedure. First, we calculate the lattice operator

$$\Phi(\vec{r},t)=\sum_{\mathbf{x}}\left[\phi\left(\vec{x},t\right)+\phi\left(\vec{x}+\vec{r},t\right)\right], \tag{1}$$

where ϕ is the plaquette operator and Φ measures the two-plaquette or two-loop component of the glueball wave function. The r dependence will be reflected in the length of links required to close the loops. From a suitable linear combinations of rotation, parity inversions and real or imaginary parts of the operators involved in Φ, one can construct glueball operators with desired quantum numbers [4, 5, 14, 15]. Since we want to explore the nature of wave functions, we focus only on the low-lying "symmetric" and "antisymmetric" scalar channels (which are the cosine and sine, respectively, of the Wilson loop in question) and tensor glueball states.

The wave function and mass are obtained from the correlation function:

$$C\left(\vec{r},t\right)=\left\langle\Phi^{\dagger}\left(\vec{r},t\right)\Phi(0,0)\right\rangle\,, \tag{2}$$

where one needs to subtract the vacuum contribution from the correlator for the 0^{++} state. The source can be held fixed, while the sink takes on the r dependence. This proves to be helpful in maintaining a good signal. The disentangling of the glueball and torelon is usually taken care of automatically by the choice of Wilson or Polyakov loops.

To increase the overlap with the lowest state and reduce the contamination from higher states, we exploit the APE link smearing techniques [16]. The procedure is implemented by an iterative replacement of the original spatial link variable by a smeared link. This results in correlations that reach their asymptotic behaviour at small time separations. In addition, the noise from ultraviolet fluctuations is reduced. The smearing parameter is fixed to 0.7 and ten iterations of the smearing process are used. To find the optimum smearing value, n, we examine the ratio (at $r=0$ and 1)

$$C(r,t+1)/C(r,t)\,,$$

which should be maximum for good ground state dominance. Using a 1×1 loop as template, the best signal is obtained with four smearing steps, with 1×1 and 2×2 loops being almost indistinguishable. At $\beta=2.0$, the signal in 1×1 showed a slow convergence with n, hence 2×2 loops were preferred for optimum overlap. A typical value, which proved to be sufficient for this case, was $n=2$.

A second pass was made to measure the optimized correlation matrices

$$C_{ij}(t)=\langle\Phi(r_i,t)\Phi(r_j,0)\rangle-\langle\Phi(r_i)\rangle\langle\Phi(r_j)\rangle\,. \tag{3}$$

Let $\psi^{(k)}$ be the radial wave function of the kth eigenstate of the transfer matrix, then

$$C_{ij}(t)=\sum_{k}\alpha_k\psi^{(k)}(r_i)\psi^{(k)}(r_j)\mathrm{e}^{-m_kt}\,. \tag{4}$$

The glueball masses and the wave functions are extracted from the Monte Carlo average of $C_{ij}(t)$ by diagonalizing the correlation matrices $C(t)$ for successive times t:

$$C(t)=\tilde{R}(t)D(t)R(t)\,, \tag{5}$$

where D is a diagonal matrix of the eigenvalues and R a rotation matrix whose columns are the eigenvectors of C. Each eigenvector of C matches an eigenstate $\psi^{(k)}(r)$ of the complete transfer matrix. As the wave function is largest at the origin, one would first determine the glueball mass with the optimal separation, and then fix that mass for all r, and extract the wave function for less optimal separations. Similar to the case of mesons [17], the wave function is expected to decrease exponentially with the r at large separations and is therefore fitted with the simple form

$$\psi(r)\equiv\mathrm{e}^{-r/r_0} \tag{6}$$

to determine the effective radius r_0. The effective mass can be read off directly from the largest eigenvalue corresponding to the lowest energy:

$$m_{\mathrm{eff}}=\log\left[\frac{\lambda_0(r=0,t=1)}{\lambda_0(r=0,t=2)}\right]. \tag{7}$$

3 Simulation results and discussion

3.1 Results at zero temperature

Most of our Monte Carlo calculations are carried out on a $16^2\times16$ lattice with periodic boundary conditions (16^2 is the space-like box and 16 is the extension in Euclidean time direction). The gauge configurations are generated using the Metropolis algorithm. After the equilibration, configurations are stored every 250 sweeps; 3000 stored configurations are used in the measurement of glueball masses. Measurements made on the stored configurations are binned into 10 blocks with each block containing an average of 300 measurements. The mean and the final errors are obtained using a single-elimination jackknife method with each bin regarded as an independent data point. Three sets of measurements were taken at $\beta=2.0, 2.25$ and 2.5. Some finite-size consistency checks are done at $\beta=2.25$ on an $20^2\times20$ lattice.

the two-link operator used in [9]. The lower dimension operator yields a linear dependence in the correlation function as opposed to an a^5 dependence for Wilson loops. This improves the glueball signal as a is reduced.

[2] The link–link operator used in [9] sums up a large number of loops; some of these loops have a zero winding number and project on glueballs – others have a non-zero winding number and project on flux states also called torelons.

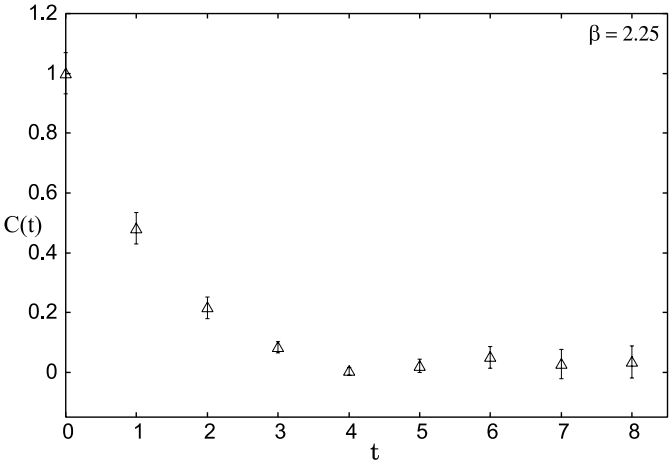

Fig. 1. Correlation function for the 0^{++} channel against t

The glueball correlation function for the 0^{++} channel against t at $\beta = 2.25$ is shown in Fig. 1. It can be seen that the expected behaviour of the correlation function is attained virtually straight away. The absolute errors in the correlation functions are expected to be independent of t for large t. Our errors are consistent with this expectation.

An effective mass plot for the $\beta = 2.5$ simulation is presented in Fig. 2. For the 0^{++} and 0^{--} channels each it was possible to find a fit region $t_{\min}$–$t_{\max}$ in which convincing plateaus were observed. The effective masses are found to be stable using different values of t in (7), which suggests that the glueball ground state is correctly projected. At $\beta = 2.5$, we noticed considerable fluctuations in the tensor mass at large t. An acceptable fit was only possible for $t = [2\text{–}5]$. To ensure the validity of our results, we compared them to those obtained using

$$m'_{\text{eff}} = \log\left[\frac{\lambda_0(t-1)-\lambda_0(t)}{\lambda_0(t)-\lambda_0(t+1)}\right]. \qquad (8)$$

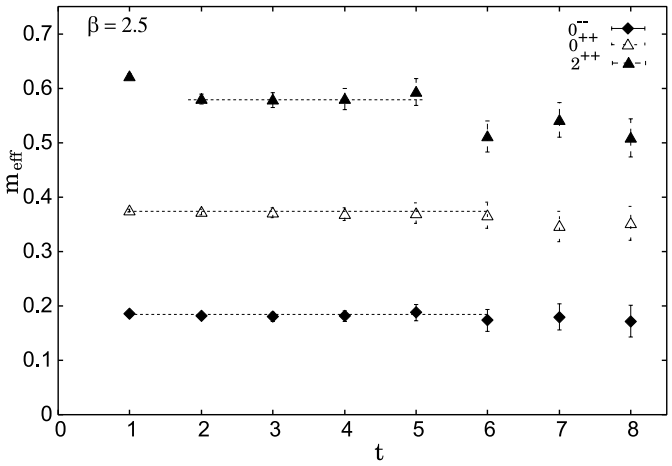

Fig. 2. Effective mass plot for scalar and tensor glueball states for $\beta = 2.5$. The *dashed horizontal lines* indicate the plateau values

It was found that the evaluations of (7) and (8) yielded results very consistent within statistical errors.

The wave functions are extracted at time separations $t = 1$ and 2. We found a little variation (less than two percent) in the eigenvectors of $C(t)$ with t, which suggests that there is no mixing with states of distinct masses. Typical plots of the wave functions, normalised to unity at the origin, for the symmetric and antisymmetric scalar glueballs, at $\beta = 2.0, 2.25$ and 2.5 are shown in Figs. 3 and 4, respectively. For guiding the eyes the Monte Carlo points of the same β-value are connected with straight lines. The scalar wave function shows the expected behaviour for all the β-values analysed here. As for the antisymmetric channel we notice the presence of negative contributions in the glueball wave function for $r > 6$ at $\beta = 2.5$. However, these contributions do not persist when the lattice size is increased from $L = 16$ to 20 (Fig. 5). This would mean that these effects are unphysical and can be described as a finite volume artifact.

For this reason we extract the effective radius of the antisymmetric state from the wave function obtained at

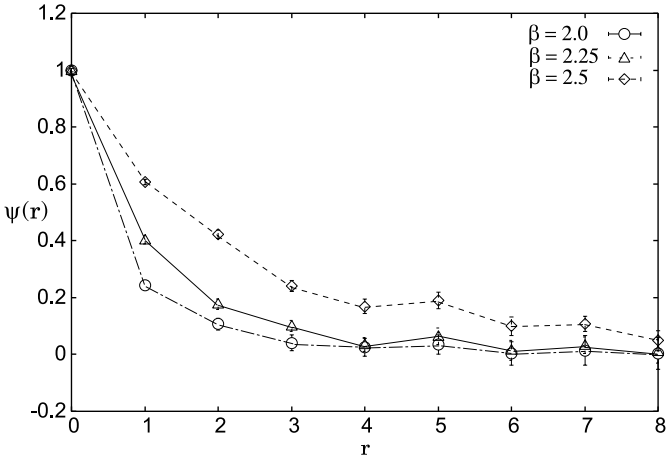

Fig. 3. Scalar 0^{++} glueball wave functions measured on a 16^3 lattice for various values of β

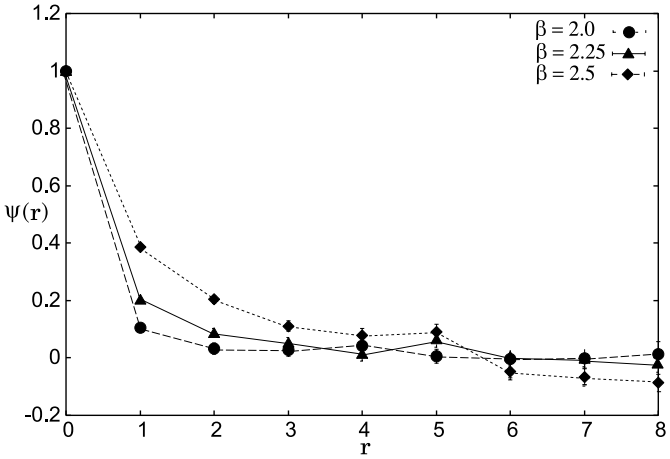

Fig. 4. Scalar 0^{--} glueball wave function on a 16^3 lattice at $\beta = 2.0, 2.25$ and 2.5

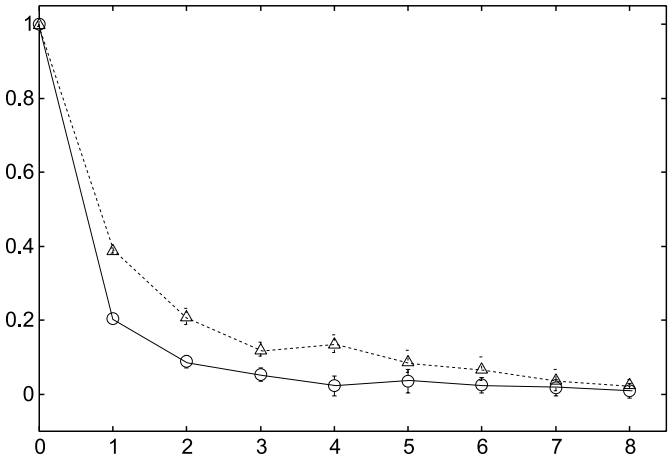

Fig. 5. Scalar 0^{--} glueball wave function on a 20^3 lattice at $\beta = 2.25$ (*open circles*) and $\beta = 2.5$ (*open triangles*)

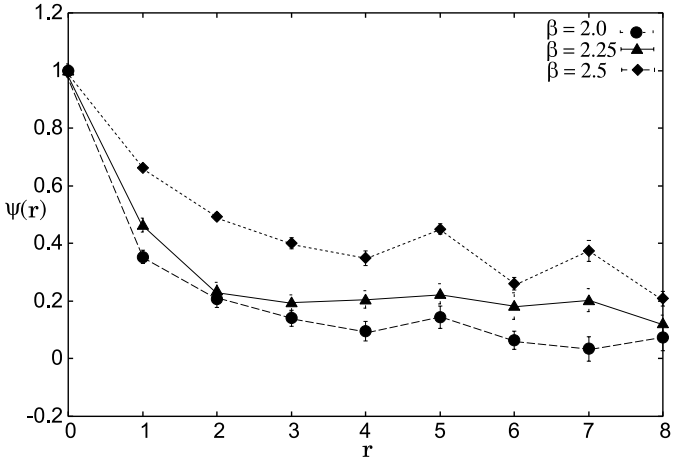

Fig. 6. Tensor glueball wave function on a 16^3 lattice at $\beta = 2.0, 2.25$ and 2.5

larger volume[3]. The symmetric scalar glueball wave function, on the other hand, barely changes sign.

Figure 6 shows the wave function for the tensor glueball, at $\beta = 2.0, 2.25$ and 2.5. The tensor wave function remains positive and shows the expected flatness. It can be seen that the tensor glueball is much more extended than the scalar one as one moves towards higher β-values. This would imply that the tensor is therefore more sensitive to the finite-size effects, which is very visible in the distortion of the wave function for large r at $\beta = 2.5$. Naively we would expect the spatial size at which we begin to encounter large finite-size effects to be related to the size of the glueball.

The expected finite-size scaling behaviour of the mass gap near the continuum critical point in this model is not known; but Weigel and Janke [18] have performed a Monte Carlo simulation for an O(2) spin model in three dimensions, which should lie in the same universality class, obtaining

$$M \approx 1.3218/L \tag{9}$$

for the magnetic gap. In order to ascertain the finite-size effect on our measurements, we performed extra simulations on a $20^2 \times 20$ lattice at $\beta = 2.25$ and 2.5. The mass and size of 0^{++} channel are almost unchanged as the lattice size increases from 16 to 20. We also find that our estimates for the tensor state are consistent with no finite volume dependence at $\beta = 2.25$. However, the tensor mass was found to increase by about 4% and the effective radius by about 7% from 16 to 20 lattices at $\beta = 2.5$. We do not have enough data to extrapolate the mass and the radius to the infinite volume limit or to check whether the difference is due to statistical errors or whether there is an incomplete convergence. Given that no mass reductions of sufficient magnitudes were found as the lattice volume is changed, none of our states could be interpreted as a torelon pair.

In order to get some quantitative information on the effective radius, the glueball wave functions are fitted in the range $3 \le r \le 8$ by the form (6). This form fits the data rather well for the scalar glueball with the best-fit estimates obtained with a $\chi^2/N_{\rm DF}$ of 0.92–0.67. Due to distortion[4] in the tensor wave function at small r at $\beta = 2.5$, a meaningful fit was possible only in the range $6 \le r \le 8$. The effective radius obtained was confirmed by examining the plateau in the ratio $\log[\psi(r)/\psi(r+1)]$. Note that our logarithmically plotted wave functions (Fig. 7) are merely illustrations.

To summarize: in the weak coupling region a spectrum of massive 0^{++}, 0^{--} and 2^{++} glueballs is indicated with

$$m(0^{--}) < m(0^{++}) < m(2^{++})\,.$$

Since there is a good signal for wave functions persisting long enough to demonstrate convergence to the asymptotic value, it seems to be reasonable to estimate the mass ratios with our present method. The estimates of the masses and r_0, in lattice units, at various β-values are shown in Tables 1–3.

Our results for lattice masses and mass ratios are generally, within statistical errors, in agreement with the existing Euclidean estimates [4, 5, 15, 19], if perhaps a little high in some places. Qualitatively our results, at zero temperature, are in agreement with the scenario of a spectrum of massive magnetic monopoles.

To extrapolate our effective radii to the continuum limit, we take the dimensionless products of sizes so that the scale, a, in which they are expressed cancels (Table 4). We choose to take products of the effective radii, $r_{0,2}/a$, to $a\sqrt{\sigma}$,

[3] The results for 16^3 lattice in Fig. 4 are shown only as an illustration. Comparison of the data for the effective mass on two lattice sizes reveals that none of our states could be interpreted as torelon pairs, since no mass reduction of sufficient magnitude was found as the lattice volume was reduced.

[4] Because of the distortion and impossible complete elimination of all the excited states, especially near $r \sim 0$, it follows that (6) holds only in the limited interval, which does not include the vicinity of $r \sim 0$.

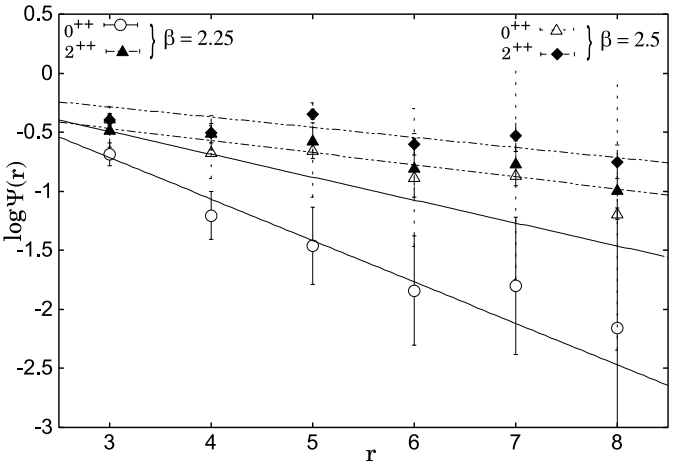

Fig. 7. The logarithmic plot of the scalar and tensor glueball wave functions at $\beta = 2.25$ and 2.5. The effective radii can be obtained from the inverse slopes of the curves

Table 1. Masses of scalar glueballs in lattice units for two spatial extensions, $L = 16$ and 20

	Mass			
	0^{++}		0^{--}	
β/L	16	20	16	20
2.0	0.803(6)		0.441(4)	
2.25	0.523(3)	0.527(3)	0.266(3)	0.261(4)
2.5	0.364(3)	0.369(2)		0.182(2)

Table 2. Sizes of scalar glueballs in lattice units for two spatial extensions, $L = 16$ and 20

	Size			
	0^{++}		0^{--}	
β/L	16	20	16	20
2.0	1.4(2)		1.0(1)	
2.25	2.75(4)	2.8(3)	2.14(4)	2.2(2)
2.5	5.1(1.0)	5.2(9)		5.0(1.0)

Table 3. Mass and size of tensor glueballs in lattice units for two spatial extensions, $L = 16$ and 20

	Mass		Size	
β/L	16	20	16	20
2.0	1.2(1)		5.0(7)	
2.25	0.82(2)	0.81(6)	9.7(1.7)	9.8(1.4)
2.5	0.544(2)	0.58(1)	10.1(2.6)	10.2(2.4)

since the string tension is our most accurately calculated quantity. As in the (3+1)D confining theories, we expect that a dimensionless product of physical quantities, such as $r_{0,2}\sqrt{\sigma}$, will approach their continuum limit with a correction of $O(a_{\rm eff}^2)$, where $a_{\rm eff}$ is the effective lattice spacing in "physical units" when the mass gap has been renormalized

Table 4. Glueball sizes in the units of string tension

β	$K(=a^2\sigma)$	$a_{\rm eff}$	$r_{0^{++}}\sqrt{\sigma}$	$r_{0^{--}}\sqrt{\sigma}$	$r_{2^{++}}\sqrt{\sigma}$
2.0	0.0508(5)	0.0856	0.31(14)	0.24(9)	1.13(18)
2.25	0.0221(3)	0.0481	0.40(17)	0.32(16)	1.14(22)
2.5	0.0119	0.0272	0.56(21)	0.50(19)	1.11(25)

to a constant [19]. The string tension, $K(=a^2\sigma)$, is obtained by using the Wilson loop averages and fitting the on-axis data with $V(r)$. In Fig. 8 we show the product $r_{0,2}\sqrt{\sigma}$ plotted against $a_{\rm eff}$. Since the products are plotted against $a_{\rm eff}$, the continuum extrapolations are simple straight lines. We notice that the product $r_{0,2}\sqrt{\sigma}$ varies only slightly over the fitting range. The non-zero lattice spacing values of the product are within 0.04–0.29 and 0.01–0.02 standard deviations of the extrapolated zero lattice spacing results for the scalar and tensor glueballs, respectively. The striking feature of this plot is the little variation of the product with $a_{\rm eff}$. This will make for very accurate and reliable continuum extrapolations. Linear extrapolations to the continuum limit yield values of 0.60 ± 0.05 and 1.12 ± 0.03, in the units of string tension, for the scalar and tensor states, respectively. In contrast to the tensor, the scalar glueball size shows significant finite-spacing errors. By setting the string tension to 420 MeV, we obtain the physical radii of 0.28(7) and 0.52(5) fm, for the scalar and tensor glueballs, respectively. Our results show the size of the tensor glueball roughly two times as large as the scalar glueball. These estimates agree with the rough estimates of glueball sizes obtained at various temperatures in [11]. This is an improvement over the estimates obtained in [9] where the predicted radius for the tensor glueball (~ 0.8 fm) was found to be four times larger than the scalar glueball radius.

3.2 Finite temperature results

To check the consistency of our method, we performed a study on an asymmetric lattice: $16^2 \times 4$ at $\beta = 2.25$. The

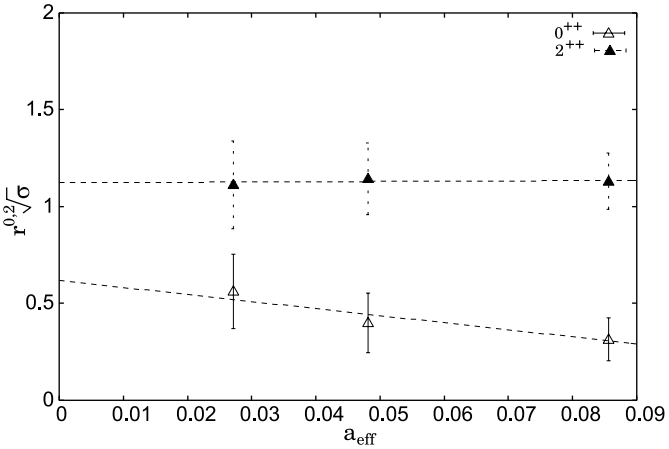

Fig. 8. Glueball radii in the units of string tension as a function of the effective spacing, $a_{\rm eff}$. Extrapolations to the continuum limit are shown as *dashed lines*

procedure itself is a straightforward extension of the procedure adopted in the previous subsection. We do not plan to study the high-temperature aspects of this model here but focus on the behaviour of the glueball mass and wave function in the deconfined region.

The physical temperature $T = 1/(aN_t)$, is given via the lattice parameters as follows:

$$T/\sqrt{\sigma} = \frac{1}{N_t\sqrt{K}}\,. \tag{10}$$

For completeness, we give a temperature estimate of 1.125 in the units of string tension. By setting the string tension to 420 MeV, we estimate a physical temperature of $T \sim 1.25T_c$, where the $T_c \sim 360$ MeV at pseudo-critical coupling $\beta_c = 1.87(2)$ [20]. One expects [21] that the high-temperature phase has a massless photon and the linear potential is replaced by the two-dimensional logarithmic Coulomb potential. This logarithmic behaviour is equivalent to a power-law dependence of the Wilson loop correlation function,

$$C(\mathbf{r}) = \langle P^\dagger(\mathbf{r})P(0)\rangle \sim |\mathbf{r}|^{-\eta(T)}\,, \tag{11}$$

with an exponent that decreases as T increases. Furthermore, since the high-temperature phase of the gauge theory corresponds to the ordered phase of the spin system, the predicted power-law behaviour of the correlation function is just like that of a two-dimensional U(1)-invariant spin system – a 2D XY model.

Figure 9 shows a plot of correlation functions versus separation. The straight line indicates the fit to the form (11). The finite temperature phase transition is visible in the change of the correlation function from exponential to power-law behaviour. Thus it becomes evident that $T > T_c$ in our simulation. It can be seen that the form (11) fits the data rather well. Nonetheless, our Monte Carlo simulations were unable to confirm that the exponent is moving towards the value of 0.25 (that of the 2D XY model [22]) predicted for the continuum theory. Our estimated value for the exponent is four times larger than the predicted value. This indicates that our β-value of 2.25 is not large enough to give us reason to hope that we are approaching continuum physics. An interesting feature to explore in this context is whether the coupling to the matter fields in the leading order ($\beta \to \infty$) calculations will move the critical exponent towards the predicted value.

In the deconfinement phase above the critical temperature, glueballs are no more elementary excitations. At high temperatures we have a plasma that behaves in bulk roughly like a free gas of quarks and gluons, thus forming a new phase, i.e., the quark–gluon plasma (QGP) phase. Above the critical temperature T_c, properties such as confinement and chiral symmetry breaking disappear. A detailed understanding of thermal glueballs gained over the last decade can be found in [11, 23–27] and the references therein. As a result, quarks and gluons are liberated and tremendous changes are expected in the mass spectrum. Figure 10 shows the scalar and tensor wave functions obtained through the same analysis as in Figs. 3 and 6. Our results indicate that no significant changes occur in the scalar and tensor wave functions. Glueball masses appear to be almost unaffected. By comparing the results at $T = 0$ and $T = 360$, we observe an effective mass reduction, $(am_G(T \sim 0) - am_G(T \sim 360))$, of about 4%, with statistical uncertainties typically on less than a percent level, for the 0^{++} and 2^{++} glueball modes. This appears to be a very small change, since we expect a rather continuous mass reduction of glueballs in the deconfined phase. This might be due to the fact that for zero momentum the power-law behaviour of the correlation function leads at short distances to the spin-wave results, which prevents us from seeing the massless excitations.

The non-vanishing effective masses would suggest the presence of glueball modes above T_c. Other work on finite temperature SU(3) [11, 23] has also confirmed the survival of correlations above T_c in the scalar and tensor colour-singlet modes. However, these studies have shown that thermal mass changes rather continuously across the critical temperature. The existence of the effective mass gives rise to the possibility that some of the nonperturbative

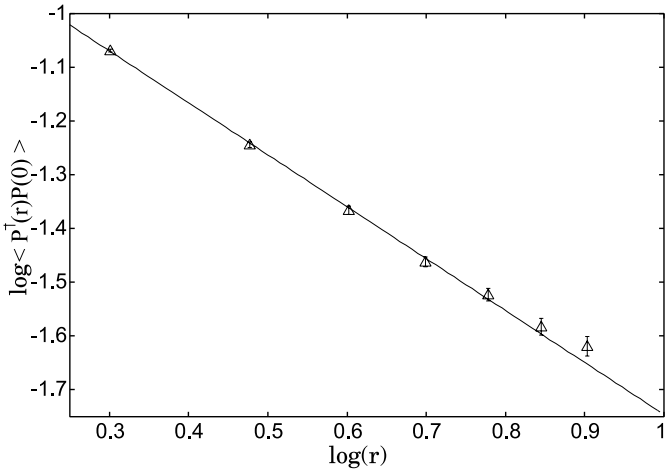

Fig. 9. The logarithmic plot of the correlation function at $\beta = 2.25$. The *straight line* indicates power-law behaviour

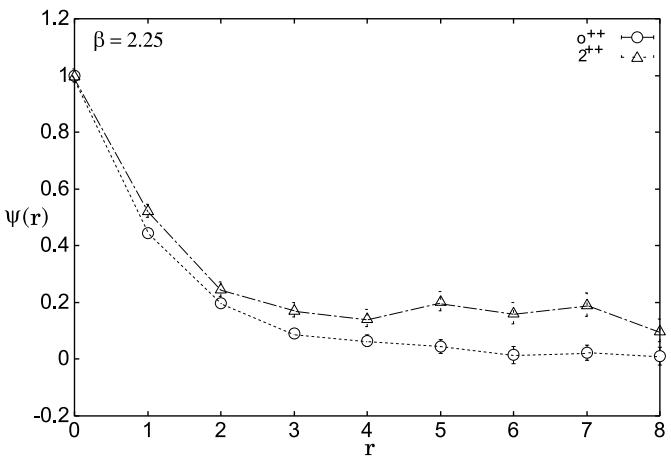

Fig. 10. Scalar and tensor glueball wave functions measured on $16^2 \times 4$ lattice at $\beta = 2.25$

effects survive in the deconfined phase, and the colour-singlet modes exist as metastable states above T_c. The metastable states in the ordered phase (large β) appear to be caused by the unusually large separation of a vortex pair, which may take many sweeps to recombine. Near the transition the number of vortices increase, and some of them begin to unbind. This eventually drives the system into a disordered phase as one moves to the region $T < T_c$.

Whether bound or metastable modes, the glueballs can decay into two or more gluons, thus acquiring a finite width, which is expected to become less negligible in the deconfined phase. Thus it becomes important to take into account the effect of width in best-fit analysis. This might also explain a very modest reduction of our masses at $T > T_c$. However, from this study, it is not possible to determine whether such colour-singlet modes really survive above T_c as metastable states. An extensive systematic analysis, of unquenched improved lattice QCD at finite temperature, along these lines is under way [28].

4 Summary and conclusion

We have studied wave functions and sizes of scalar and tensor glueballs using an improved 3-dimensional U(1) lattice model. In this preliminary study we take a more direct approach to the problem; instead of fixing a gauge or a path for the gluons, we measure the correlation functions from our lattice operators from spatially connected Wilson loops which, being the expectation values of closed-loop paths, are gauge invariant. This approach has the advantage that the disentangling of the glueball and torelon is usually taken care of automatically by the choice of Wilson or Polyakov loops. We observed that the size of the tensor glueball is roughly two times larger than the size of the scalar glueball. We believe that our estimates are more reliable than the results obtained in [9], where the size of the tensor glueball was found to be ~ 0.8 fm, four times as large as its scalar counterpart. The predicted zero lattice spacing results are not actually found by extrapolation to zero lattice spacing, but are obtained instead from calculations at β of 2.2 of glueball size, with no accurate representation of the effect of the absence of extrapolation. Also the results were of limited interest because of their manifest dependence on the gauge chosen and the problem of disentangling of the glueballs and torelons.

Finally, for completeness, we extended our method to measure the wave function and mass for a finite temperature deconfinement phase. For the lowest 0^{++} and 2^{++} glueballs, no significant mass reduction was observed in the deconfined phase, while the wave functions remain almost unchanged. The existence of the effective mass indicates that colour-singlet modes may survive in the deconfined phase as metastable states. In such a case glueball decay and decay width, as a spectral component, in the deconfinement phase are the most feasible candidates for a more reliable analysis for the future studies.

Acknowledgements. We are grateful to D. Leinweber and C. Hamer for a number of valuable suggestions, which provided the impetus for much of this work. We are also grateful for access to 128 node DeepSuper -21C computing facility at the Shenzhen University. This work was supported by the Guangdong Provincial Ministry of Education and Jinan University.

References

1. C.J. Morningstar, M.J. Peardon, Phys. Rev. D **60**, 034509 (1999)
2. C.J. Morningstar, M.J. Peardon, Phys. Rev. D **56**, 4043 (1997)
3. A. Vaccarino, D. Weingarten, Phys. Rev. D **60**, 114501 (1999)
4. M. Teper, Phys. Lett. B **397**, 223 (1997)
5. M. Teper, Phys. Rev. D **59**, 014512 (1998)
6. N.H. Shakespeare, H.D. Trottier, Phys. Rev. D **59**, 014502 (1999)
7. UKQCD Collaboration, G. Bali et al., Phys. Lett. B **309**, 378 (1993)
8. T. DeGrand, Phys. Rev. D **36**, 182 (1987)
9. P. de Forcrand and K.-F. Liu, Phys. Rev. Lett. **69**, 245 (1992)
10. G. Boyd, et al., Nucl. Phys. B **469**, 419 (1996)
11. N. Ishii, H. Suganuma, H. Matsufura, Phys. Rev. D **66**, 094506 (2002)
12. C. Alexandrou, P. de Forcrand, A. Tsapalis, Phys. Rev. D **66**, 094503 (2002)
13. S. Sakai, A. Nakamura, T. Saito, Nucl. Phys. Proc. Suppl. **106**, 543 (2002)
14. M. Loan et al., Phys. Rev. D **68**, 034504 (2003)
15. M. Loan, C. Hamer, Phys. Rev. D **70**, 014504 (2004)
16. M. Albanese et al., Phys. Lett. B **192**, 163 (1987)
17. B. Velikson, D. Weingarten, Nucl. Phys. B **249**, 433 (1985)
18. M. Weigel, W. Janke, Phys. Rev. Lett. **82**, 2318 (1999)
19. M. Loan, T. Byrnes, C. Hamer, Eur. Phys. J. C **31**, 397 (2003)
20. M. Chernodub, E.-M. Illgenfritz, A. Schiller, Phys. Rev. D **64**, 054507 (2001)
21. B. Svetitsky, L. Yaffe, Nucl. Phys. B **210**, 423 (1982)
22. J. Tobochnik, G. Chester, Phys. Rev. B **20**, 3761 (1979)
23. C. DeTar, J. Kogut, Phys. Rev. Lett. **59**, 399 (1987)
24. S. Datta, S. Gupta, Nucl. Phys. B **534**, 392 (1998)
25. S. Datta, S. Gupta, Phys. Rev. D **67**, 054503 (2003)
26. P. Bialas, A. Morel, B. Petersson, Nucl. Phys. B **704**, 208 (2005)
27. A. Hart, M. Laine, O. Philipsen, Nucl. Phys. B **586**, 443 (2000)
28. M. Loan, C. Hamer, R. Bursill, in preparation